Chemistry & Biology
Article

A Mitochondria-Targeted Macrocyclic Mn(II) Superoxide Dismutase Mimetic

Geoffrey F. Kelso,[1] Andrej Maroz,[2] Helena M. Cochemé,[3,4] Angela Logan,[3] Tracy A. Prime,[3] Alexander V. Peskin,[5] Christine C. Winterbourn,[5] Andrew M. James,[3] Meredith F. Ross,[3] Sally Brooker,[6] Carolyn M. Porteous,[7] Robert F. Anderson,[2] Michael P. Murphy,[3,*] and Robin A.J. Smith[1]
[1]Centre for Green Chemistry, Monash University, Victoria 3800, Australia
[2]School of Chemical Sciences, The University of Auckland, Private Bag 92019, Auckland 1142, New Zealand
[3]Medical Research Council Mitochondrial Biology Unit, Hills Road, Cambridge CB2 0XY, UK
[4]Department of Genetics, Evolution, and Environment, Institute of Healthy Ageing, University College London, Gower Street, London WC1E 6BT, UK
[5]Department of Pathology, University of Otago Christchurch, P.O. Box 4345, Christchurch, New Zealand
[6]Department of Chemistry
[7]Department of Biochemistry
University of Otago, PO Box 56, Dunedin 9054, New Zealand
*Correspondence: mpm@mrc-mbu.cam.ac.uk
http://dx.doi.org/10.1016/j.chembiol.2012.08.005

SUMMARY

Superoxide ($O_2^{\bullet-}$) is the proximal mitochondrial reactive oxygen species underlying pathology and redox signaling. This central role prioritizes development of a mitochondria-targeted reagent selective for controlling $O_2^{\bullet-}$. We have conjugated a mitochondria-targeting triphenylphosphonium (TPP) cation to a $O_2^{\bullet-}$-selective pentaaza macrocyclic Mn(II) superoxide dismutase (SOD) mimetic to make MitoSOD, a mitochondria-targeted SOD mimetic. MitoSOD showed rapid and extensive membrane potential-dependent uptake into mitochondria without loss of Mn and retained SOD activity. Pulse radiolysis measurements confirmed that MitoSOD was a very effective catalytic SOD mimetic. MitoSOD also catalyzes the ascorbate-dependent reduction of $O_2^{\bullet-}$. The combination of mitochondrial uptake and $O_2^{\bullet-}$ scavenging by MitoSOD decreased inactivation of the matrix enzyme aconitase caused by $O_2^{\bullet-}$. MitoSOD is an effective mitochondria-targeted macrocyclic SOD mimetic that selectively protects mitochondria from $O_2^{\bullet-}$ damage.

INTRODUCTION

The mitochondrial respiratory chain is a major source of superoxide ($O_2^{\bullet-}$), which can go on to form other reactive oxygen species (ROS), such as hydrogen peroxide (H_2O_2), the hydroxyl radical ($^{\bullet}OH$), and peroxynitrite ($ONOO^-$) (Murphy, 2009). The production of $O_2^{\bullet-}$ and derived ROS leads to oxidative damage that disrupts mitochondrial function and thereby contributes to a range of pathologies, including neurodegenerative diseases, diabetes, and ischemia-reperfusion injury (Finkel, 2005). Mitochondrial ROS production is also an important component of redox signaling (Collins et al., 2012; Murphy, 2009). To protect against oxidative damage and explore redox signaling pathways, mitochondria-targeted antioxidants have been developed that comprise a lipophilic triphenylphosphonium (TPP) cation conjugated to an antioxidant moiety (Murphy and Smith, 2007; Smith et al., 2011). The large lipophilic surface of the TPP cation enables such compounds to move rapidly through biological membranes, while their positive charge causes them to be accumulated several 100-fold inside mitochondria in vivo driven by the large membrane potential of up to 180 mV (negative inside) (Ross et al., 2005). This dramatic mitochondrial accumulation makes targeted antioxidants far more protective against oxidative damage than untargeted equivalents in cultured cells, in animal models of pathologies, and in human clinical trials (Gane et al., 2010; Murphy and Smith, 2007, 2010; Snow et al., 2010). A targeted version of ubiquinone (MitoQ) is the most extensively studied of these mitochondria-targeted antioxidants (Kelso et al., 2001; Murphy and Smith, 2007, 2010). Many other antioxidants have been targeted to mitochondria by conjugation to the TPP cation, including vitamin E (Smith et al., 1999), plastoquinone (Skulachev et al., 2009), Ebselen (Filipovska et al., 2005), lipoic acid (Brown et al., 2007), nitroxides (Dhanasekaran et al., 2005; Trnka et al., 2008), and nitrones (Murphy et al., 2003). The central role of $O_2^{\bullet-}$ in mitochondrial metabolism requires the development of a mitochondria-targeted antioxidant that is selective for $O_2^{\bullet-}$. A number of mitochondria-targeted antioxidants do react with $O_2^{\bullet-}$. The nitroxide MitoTEMPOL has SOD activity in vitro but is rapidly reduced to the hydroxylamine within mitochondria, and thus its protective properties are not attributable to its reactions with $O_2^{\bullet-}$ (Trnka et al., 2008). The related molecule, incorporating an amide-linked TPP, MitoTEMPO, also has SOD activity in vitro, as well as protective effects in vivo (Dikalova et al., 2010); however, its biological activity is unlikely to be due to its SOD activity as it is also reduced to the hydroxylamine in vivo (Soule et al., 2007). The mitochondria-targeted nitroxide Mito-Carboxy Proxyl (MitoCP) protects against oxidative damage to mitochondria far more effectively than the untargeted version and has a $O_2^{\bullet-}$ dismutation rate of $\sim 10^5$ M^{-1} s^{-1} in vitro (Dhanasekaran et al., 2005); however, it is likely that protection by MitoCP is largely due to other antioxidant reactions

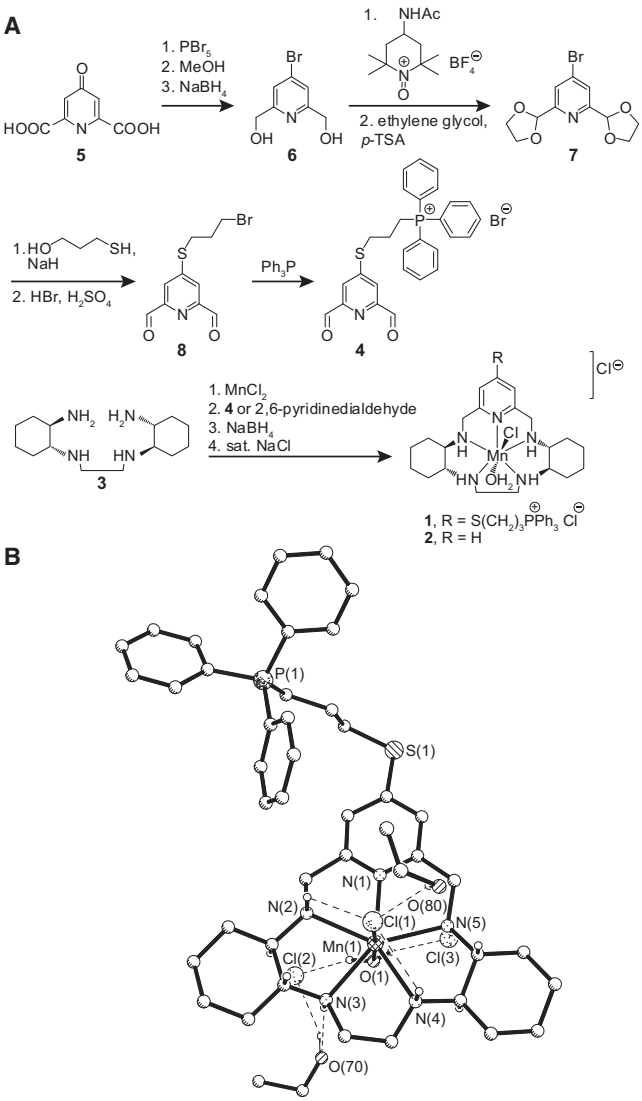

Figure 1. Synthesis and Structure of MitoSOD

(A) MitoSOD (**1**) was obtained by Mn(II) template cyclization of the tetraamine **3** and the 2,6-pyridine dialdehyde derivative **4** followed by in situ borohydride reduction. Compound **4** was obtained from chelidamic acid (**5**) via the bromodiol (**6**) and oxidized derivatives (**7**, **8**). M40403 (**2**) was obtained similarly from **3** and 2,6-pyridine dialdehyde.

(B) A projection view of MitoSOD $[Mn(II)(L^{+})(Cl)(OH_2)](Cl)_2 \cdot CH_3CH_2OH$ (**1**$(OH_2)\cdot CH_3CH_2OH$) derived from single crystal X-ray diffraction data. The dashed lines represent hydrogen bonds. O(70) and O(80) represent the oxygen atoms of half occupancy ethanol molecules. O(1) represents the oxygen atom of a coordinated H_2O molecule. Only the major occupancy site of Cl(2) is shown. Hydrogen atoms, other than those on chiral centers or involved in hydrogen bonding, have been omitted for clarity.

See also Tables S1–S3.

of this nitroxide and its hydroxylamine reaction products (Kagan et al., 2007). A TPP-conjugated version of the salen-Mn(III) compound EUK-134 has only limited protection against oxidative damage; however, its uptake into mitochondria was not demonstrated (Dessolin et al., 2002). Furthermore, as this class of Mn(III) complex has both SOD and catalase mimetic activity, it would be difficult to distinguish the effects of depleting $O_2^{\cdot-}$ from that of degrading H_2O_2 (Doctrow et al., 1997).

Although there are a number of antioxidant compounds targeted to mitochondria that do react with $O_2^{\cdot-}$, they are not selective, and furthermore their rates of reaction with $O_2^{\cdot-}$ are typically $\sim 10^5\ M^{-1}s^{-1}$, considerably lower than that of MnSOD, the mitochondrial SOD isoform ($\sim 2 \times 10^9\ M^{-1}\ s^{-1}$; Cadenas and Davies, 2000). As the biological effects of these compounds are unlikely to be due solely to their reactivity with $O_2^{\cdot-}$, they cannot be used to infer the role of mitochondrial $O_2^{\cdot-}$ in oxidative damage or redox signaling. Consequently, there is a need to modulate mitochondrial $O_2^{\cdot-}$ selectively using a synthetic mitochondria-targeted SOD mimetic. The importance of this challenge is supported by the observation that selectively decreasing mitochondrial $O_2^{\cdot-}$ by overexpressing MnSOD enzyme gives therapeutically relevant protection in animal models of disease (Chen et al., 1998) and modulates redox signaling (Kim et al., 2004; Murphy, 2009). To address this need, we have synthesized a mitochondria-targeted SOD mimetic, MitoSOD (**1**), based on the established pentaaza macrocyclic Mn(II) SOD mimetic M40403 (**2**) (Salvemini et al., 1999, 2002) (Figure 1A). This molecule was chosen from a wide variety of known Mn-based SOD mimetics (Batinić-Haberle et al., 2010; Iranzo, 2011) because it is an effective SOD mimetic in vitro and has been shown to be stable and protective in vivo (Thompson et al., 2010). Our previous study of M40403 reaction kinetics using pulse radiolysis demonstrated that in a phosphate environment it catalyzes $O_2^{\cdot-}$ dismutation to H_2O_2 with $k_{cat} = 3.55 \times 10^6\ M^{-1}\ s^{-1}$ at 22°C (pH 7.4) (Maroz et al., 2008), in good agreement with the value more recently reported using the stopped flow method ($2.3 \pm 0.1 \times 10^6\ M^{-1}s^{-1}$ [pH 7.4], 21°C; Friedel et al., 2012). The catalytic SOD cycle involves an initial fast reaction of M40403 with $O_2^{\cdot-}$ ($k_1 = 9.0 \pm 0.5 \times 10^7\ M^{-1}\ s^{-1}$, 22°C [pH 8.0]) to produce a $[Mn^{III}(L)Cl_nO_2]^{(2-n)+}$ intermediate containing a coordinated peroxide (Maroz et al., 2008). This rapid reaction underlies the $O_2^{\cdot-}$ selectivity of M40403 and its lack of reactivity with other ROS, such as $ONOO^-$, H_2O_2 or HOCl (Salvemini et al., 2002). Whereas a triethylenetetraamine analog of M40403 reacts with NO (Filipović et al., 2008, 2010), the rate constant is about 10^5 times smaller than that for the initial reaction of M40403 with $O_2^{\cdot-}$. The SOD mimetic Mn(III) metalloporphyrins (Batinić-Haberle, 2002) have high rates of reaction with $O_2^{\cdot-}$, but they are not chemoselective as they also react at comparable rates with $ONOO^-$ and $CO_3^{\cdot-}$ (Salvemini et al., 2002). The Mn(III)-salen compounds have SOD activity but also show catalase activity (Doctrow et al., 1997). Here, we report the synthesis of a mitochondria-targeted SOD mimetic, MitoSOD, that is accumulated by mitochondria and selectively degrades mitochondrial $O_2^{\cdot-}$, protecting against oxidative damage. The chemical and biological properties of MitoSOD establish an opportunity to control and assess $O_2^{\cdot-}$ production within mitochondria.

RESULTS AND DISCUSSION

Design and Synthesis of MitoSOD

MitoSOD was designed by attaching a TPP lipophilic cation to the pyridine ring of M40403 so as to drive its selective accumulation and ultimate dismutation of $O_2^{\cdot-}$ within mitochondria. MitoSOD (**1**) and the untargeted SOD mimetic macrocycle

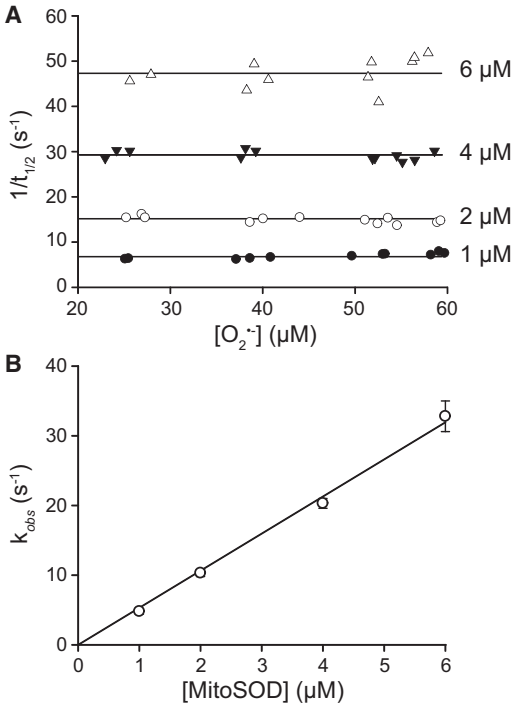

Figure 2. Kinetics of MitoSOD Activity Measured by Pulse Radiolysis

(A) Kinetic plots showing the dependence of the reciprocal first half-life of $O_2^{\bullet-}$ on the concentration of $O_2^{\bullet-}$ at pH 8.0, measured at 270 nm, in the absence (control) and with increasing concentrations of MitoSOD. Data were obtained following the pulse radiolysis (35–100 Gy in 1.5 μs) of oxygen-saturated aqueous solutions containing sodium formate (10 mM), phosphate buffer (10 mM), and EDTA (0.1 mM).

(B) Dependence of rate constants for the reaction of MitoSOD with $O_2^{\bullet-}$ (derived from intercepts of A) on the concentration of MitoSOD. The slope of the fitted line provides the value for k_{cat} shown in Table 1.

M40403 (**2**) were synthesized as shown in Figure 1A, and the structure of MitoSOD was determined by X-ray crystallography (Figure 1B). The structure of MitoSOD was similar to that of M40401, the active dimethyl analog of M40403 (Aston et al., 2001), and the addition of a TPP cation appendage did not distort the macrocycle conformation, which is crucial for SOD-mimetic activity.

Kinetics of Superoxide Dismutation by MitoSOD

To determine whether MitoSOD was an effective SOD mimetic, we measured its rate of catalytic dismutation of $O_2^{\bullet-}$. This was done by generating $O_2^{\bullet-}$ (1–60 μM in 1.5 μs) by the pulse radiolysis of phosphate buffer (pH 7.4 or 8.0), containing sodium formate and EDTA, and measuring the decay of $O_2^{\bullet-}$ spectrophotometrically (Bielski et al., 1985). In the absence of MitoSOD, $O_2^{\bullet-}$ decay followed mixed first- and second-order kinetics, which is interpreted as the spontaneous dismutation of $O_2^{\bullet-}$ (k_{self}) and background catalytic decomposition, presumably by trace metal impurities. When [MitoSOD] ≫ [$O_2^{\bullet-}$], the decay of $O_2^{\bullet-}$ was predominantly pseudo-first-order because of the fast reaction of the macrocycle with $O_2^{\bullet-}$ ($k_1 = 1.57 \pm 0.04 \times 10^8\ M^{-1}\ s^{-1}$ [pH 8.0]). We propose that the product of this reaction is a $[Mn^{III}(L\text{-}TPP)Cl_nO_2]^{(3-n)+}$ intermediate containing a coordinated peroxide, as has been demonstrated for the parent M40403 macrocycle (Maroz et al., 2008). When catalytic (1–6 μM) amounts of MitoSOD were present at pH 8.0, reflecting that within mitochondria, the rate of $O_2^{\bullet-}$ decay (20–60 μM) was considerably faster compared to $O_2^{\bullet-}$ alone and also followed mixed first- and second-order kinetics, which indicated that $O_2^{\bullet-}$ was decaying by spontaneous (k_{self}) and MitoSOD-catalyzed (k_{obs}) dismutation. To determine k_{obs}, the first half-life ($t_{1/2}$) of $O_2^{\bullet-}$ decay was measured over a range of $O_2^{\bullet-}$ concentrations with different concentrations of MitoSOD, and then plots of $1/t_{1/2}$ versus [$O_2^{\bullet-}$] were constructed (Figure 2A), and values of k_{obs} were calculated from the y-intercepts, as previously described (Anderson et al., 2003). A plot of k_{obs} versus MitoSOD concentration was linear (Figure 2B), demonstrating that the decay of $O_2^{\bullet-}$ was first order in both $O_2^{\bullet-}$ and MitoSOD, indicative of catalytic dismutation. The rate constant for the catalyzed dismutation (k_{cat}) was calculated from the slope of the fitted function and is presented in Table 1 along with the value measured at pH 7.4 and our previously determined values for M40403 (Maroz et al., 2008). MitoSOD and M40403 were found to have similar SOD activities, but that of MitoSOD decreased at pH 7.4 (Table 1), presumably because of a pH-dependent effect of the (3-mercaptopropyl) triphenylphosphonium substituent on the reactivity of the intermediate Mn(III) complex. In summary, MitoSOD is an effective SOD mimetic, and its initial fast reaction with $O_2^{\bullet-}$ underlies the selectivity for this ROS in a biological environment.

Table 1. Superoxide Dismutase Activity of MitoSOD and M40403 Measured by Pulse Radiolysis

	$k_{cat} \times 10^{-6}$ ($M^{-1}\ s^{-1}$)	
Compound	pH 7.4	pH 8.0
MitoSOD	2.5 ± 0.2	5.3 ± 0.2
M40403	3.6 ± 0.2	2.6 ± 0.2

To evaluate whether MitoSOD could also act as a SOD mimetic under the steady-state $O_2^{\bullet-}$ flux that occurs within mitochondria, $O_2^{\bullet-}$ was generated continuously by xanthine oxidase (XO) and monitored by the rate of cytochrome *c* reduction. The reactivity of MitoSOD with $O_2^{\bullet-}$ was determined from its competition with cytochrome *c* reduction (Figures 3A and 3B) (Loschen et al., 1974). These experiments showed that MitoSOD effectively blocked cytochrome *c* reduction in a dose-dependent manner by competing for $O_2^{\bullet-}$, whereas a control TPP cation without any bioactive cargo, methyltriphenylphosphonium bromide (TPMP), was ineffective (Figures 3A and 3B). A plot of the reciprocal of the cytochrome *c* reduction rate versus compound concentration from Figure 3B was linear and, by slope comparison, indicated that 1.1 nmol MitoSOD corresponded to 1 U Cu, ZnSOD. In a separate approach, we assessed the ability of MitoSOD to intercept a steady-state flux of $O_2^{\bullet-}$ using the WST-1 reduction assay (Peskin and Winterbourn, 2000). Here, we found that to get 50% inhibition of WST-1 reduction required 2.4 ± 0.1 ng (0.14 pmol) Cu,ZnSOD monomer; 96 ± 28 ng (197 pmol) M40403; and 10 ± 5 ng (20 pmol) MitoSOD (means ± SD, n = 3). So by this assay, MitoSOD is ~10-fold more effective than M40403 and ~140-fold less effective than Cu,ZnSOD.

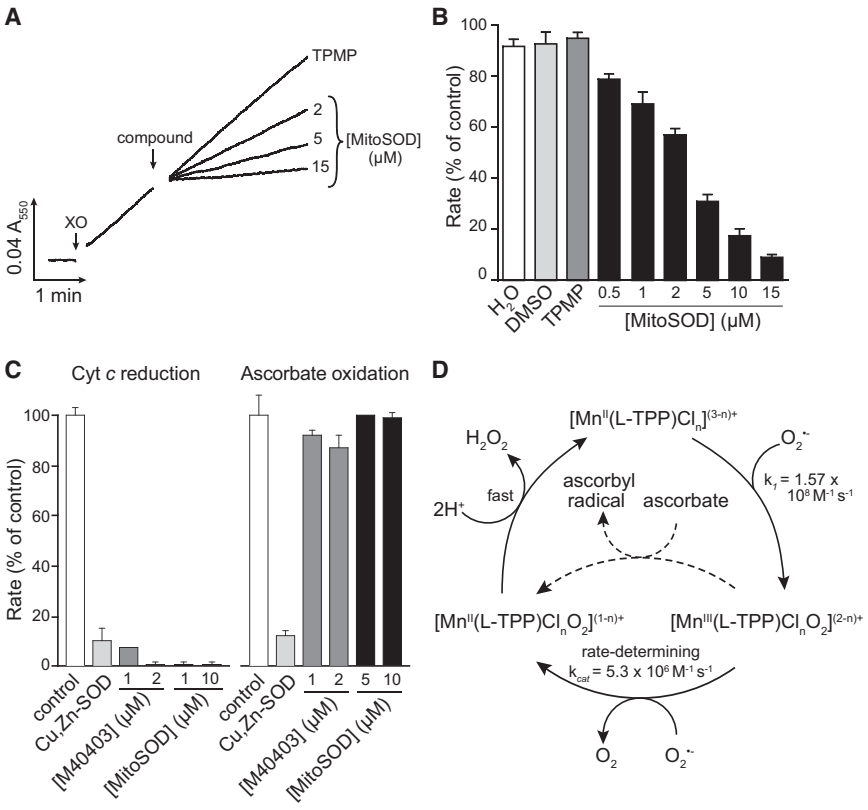

Figure 3. Steady-State Activity of MitoSOD

(A) $O_2^{\bullet-}$ was generated by the addition of xanthine oxidase (XO). Where indicated (second arrow) MitoSOD (2–15 μM) or control compound (methyltriphenylphosphonium bromide; TPMP, 15 μM) was added, and the rate of reduction of cytochrome *c* by $O_2^{\bullet-}$ was assessed at 550 nm. Data shown are typical traces of experiments repeated in triplicate.

(B) The slope of cytochrome *c* reduction by XO/hypoxanthine in the presence of the indicated additions was divided by that in the absence of additions to give the relative SOD activity. Data are means ± SD, n = 3.

(C) Ascorbate oxidation and cytochrome *c* reduction in the presence of M40403 and MitoSOD. A flux of $O_2^{\bullet-}$ was generated by addition of XO and acetaldehyde (10 mM), and then Cu,ZnSOD (60 nM) or various concentrations of M40403 and MitoSOD were added. Then either cytochrome *c* was added and its rate of reduction was monitored at 550 nm, or ascorbate 30 μM was added and its rate of oxidation was monitored at 266 nm. Note that MitoSOD has a greater effect on cytochrome *c* reduction in (C) than in (A) and (B) because the flux of superoxide generated is about 3-fold lower in (C). Data are means ± ranges for 2–3 determinations.

(D) The proposed mechanism for the MitoSOD-catalyzed dismutation of $O_2^{\bullet-}$ is shown. In addition, an alternative path for the rate-limiting reduction of the Mn(III) species to Mn(II) by ascorbate is shown as a dashed line.

The Mn(III) porphyrin SOD mimetics were more effective at protecting against $O_2^{\bullet-}$ within cells than their in vitro SOD activity would predict (Faulkner et al., 1994). Because SOD catalysis by M40403 involves a rate-limiting reduction of an intermediate Mn(III) complex by another $O_2^{\bullet-}$ (Maroz et al., 2008), in a biological environment this intermediate could be reduced by reductants other than $O_2^{\bullet-}$. The mitochondrial matrix contains a significant amount of ascorbate (~0.5 mM) (Li et al., 2001); therefore, we indirectly assessed ascorbate reduction of the MitoSOD and M40403 Mn(III) intermediates by measuring ascorbate oxidation in the presence of SOD mimetic and $O_2^{\bullet-}$ (Figure 3C). As expected from the rate constant (3×10^5 $M^{-1}s^{-1}$) for the direct reaction of ascorbate with $O_2^{\bullet-}$ (Gotoh and Niki, 1992), when we generated $O_2^{\bullet-}$ by XO there was rapid oxidation of ascorbate. However, in contrast to the more catalytically active Cu, Zn SOD enzyme, neither MitoSOD nor M40403 decreased ascorbate oxidation (Figure 3C). This result suggests that in the presence of $O_2^{\bullet-}$, the Mn(III) intermediate within the catalytic cycle of MitoSOD or M40403 SOD activity oxidizes ascorbate (Figure 3D), as the rate constants for the initial reaction of $O_2^{\bullet-}$ with MitoSOD (k_1 = 1.38 ± 0.08 × 10^8 [pH 7.2]) or M40403 (8.9 ± 0.4 × 10^7 M^{-1} s^{-1} [pH 7.4]) (Maroz et al., 2008) are much higher than that of $O_2^{\bullet-}$ with ascorbate. Neither GSH nor NADH were able to accelerate the steady-state dismutation of $O_2^{\bullet-}$ by MitoSOD when measured as in Figure 3A (data not shown), suggesting these biological-reducing agents do not react with the Mn(III) intermediate. In summary our results suggest that in a biological environment MitoSOD and M40403 will selectively decompose $O_2^{\bullet-}$ by acting as both a SOD mimetic and as an ascorbate/superoxide oxidoreductase catalyst, thereby enhancing their ability to catalytically decompose $O_2^{\bullet-}$.

The overall kinetic scheme supported by these data and our previous study (Maroz et al., 2008) is presented in Figure 3D. To summarize, MitoSOD-catalyzed dismutation of $O_2^{\bullet-}$ involves an initial fast inner sphere oxidation of the macrocycle by $O_2^{\bullet-}$ (k_1 = 1.57 ± 0.04 × 10^8 M^{-1} s^{-1} [pH 8.0]) to form an $[Mn^{III}(L\text{-}TPP)Cl_nO_2]^{(2-n)+}$ intermediate that then undergoes a relatively slow reduction (k_{cat}) with further $O_2^{\bullet-}$ to give a putative short-lived $[Mn^{II}(L\text{-}TPP)Cl_nO_2]^{(1-n)+}$ intermediate that rapidly decomposes to the parent $[Mn^{II}(L\text{-}TPP)Cl_n]^{(3-n)+}$ macrocycle (Maroz et al., 2008). The essential observation is that MitoSOD has similar SOD activity to M40403, demonstrating the structural modification incorporated to facilitate transport into mitochondria did not disrupt the desired catalytic activity. In addition, MitoSOD and M40403 catalyze the reduction of $O_2^{\bullet-}$ to H_2O_2 using electrons from ascorbate (Faulkner et al., 1994), as is illustrated in Figure 3D. We conclude that MitoSOD should be effective at selectively catalyzing the degradation of $O_2^{\bullet-}$ within mitochondria.

Stability, Charge, and Hydrophobicity of MitoSOD

To be biologically useful MitoSOD has to be stable. In 1 M HCl MitoSOD rapidly dissociated to metal-free macrocycle and Mn(II), as detected by positive ion electrospray mass spectrometry (data not shown). The rates of MitoSOD dissociation from pH 3.8 to 4.3 were modest and had a linear dependence on $[H^+]$ (Figures S1A and S1B available online) (Aston et al., 2001), as reported for M40403 (Salvemini et al., 1999). This gave k_{dis}

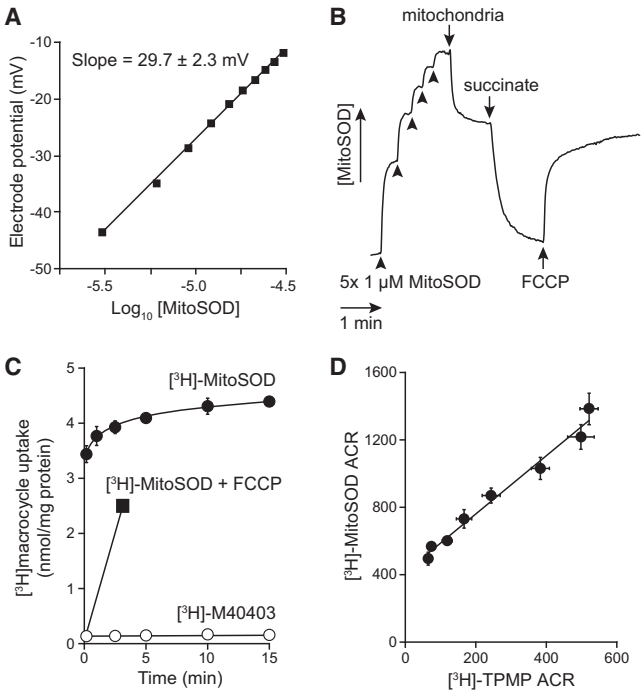

Figure 4. Uptake of MitoSOD by Energized Mitochondria

(A) The ion-selective electrode response to ten sequential aliquots of 3 μM MitoSOD at 30°C was plotted versus $\log_{10}$[MitoSOD]. The straight line represents a linear function fitted to the data by least-squares regression analysis.

(B) Ion-selective electrode measurement of MitoSOD uptake by energized mitochondria. Incubation medium supplemented with rotenone (4 μg ml^{-1}) was added to the incubation chamber at 37°C, and the electrode was then calibrated by five sequential additions of 1 μM MitoSOD. Liver mitochondria (2 mg protein ml^{-1}) were then added, followed by succinate (2 mM) and FCCP (500 nM) where indicated.

(C) Time dependence of uptake of [^{3}H]MitoSOD and [^{3}H]M40403 by isolated mitochondria. Rat liver mitochondria were incubated with 5 μM [^{3}H]MitoSOD or [^{3}H]-M40403 at 25°C and the uptake determined at various times. The data are means of three separate experiments ± SEM. For the FCCP experiment, 500 nM FCCP was present.

(D) The effect of the mitochondrial membrane potential on the uptake of [^{3}H]-MitoSOD. Mitochondria were incubated with 800 nM MitoSOD and 1 μM TPMP and supplemented with 1–16 mM malonate or FCCP (330 nM). Then either 200 nM [^{3}H]MitoSOD or 100 nM [^{3}H]TPMP was added, and the ACR values of [^{3}H]MitoSOD or [^{3}H]TPMP were determined in parallel. The data are means of duplicate incubations of three separate experiments ± SEM. The equation of the line is $y = 1.727X + 415$, $R^2 = 0.98$.

See also Figure S1.

for MitoSOD = 2.64 ± 0.11 × 10^{-2} M^{-1} s^{-1} at 18°C, corresponding to a half-life at pH 7.2 of ≈13 years. This was corroborated by incubating 150 μM MitoSOD at pH 8.0, which, by high-performance liquid chromatography monitoring, showed that it was stable for at least two weeks. In contrast, at pH 1.0 the half-life is ~3.8 min. Therefore, MitoSOD is stable under most biological conditions but would dissociate rapidly in stomach acid.

For MitoSOD to act as a mitochondria-targeted antioxidant, it must pass easily through phospholipid bilayers, which will depend critically on its overall charge. The Mn(II) cation is bound to the macrocycle (L-TPP) and 0, 1, or 2 chloro ligands, giving three possible species: $[Mn^{II}(L\text{-}TPP)]^{3+}$, $[Mn^{II}(L\text{-}TPP)Cl]^{2+}$, or $[Mn^{II}(L\text{-}TPP)Cl_2]^{+}$. The molar conductivity of MitoSOD in water was 294 S cm^2 mol^{-1} at 20°C, indicative of a 1:3 electrolyte (Feltham and Hayter, 1964), indicating that both chloro ligands and the TPP chloride counter anion dissociated to give $[Mn^{II}(L\text{-}TPP)]^{3+}$. However, when MitoSOD in 90% acetonitrile was infused into a mass spectrometer, only species at m/z = 391 and 817 were detected, corresponding to $[Mn^{II}(L\text{-}TPP)Cl]^{2+}$ and $[Mn^{II}(L\text{-}TPP)Cl_2]^{+}$, and there was no peak at m/z = 249 as expected for $[Mn^{II}(L\text{-}TPP)]^{3+}$ (Figure S2A). This suggests that under biological conditions of [Cl^-] (~120 mM), the $[Mn^{II}(L\text{-}TPP)Cl]^{2+}$ and $[Mn^{II}(L\text{-}TPP)Cl_2]^{+}$ forms will predominate. To extend this we assessed the effect of [MitoSOD] on the potential of an ion-selective electrode sensitive to TPP cations (Asin-Cayuela et al., 2004). In 120 mM KCl, the electrode potential was a linear function of $\log_{10}$[MitoSOD] with a slope of 29.7 ± 2.3 mV/decade (Figure 4A), consistent with a Nernstian response of the electrode to a dication. Together, these data suggest that under biological conditions the predominant form of MitoSOD is $[Mn^{II}(L\text{-}TPP)Cl]^{2+}$ although $[Mn^{II}(L\text{-}TPP)Cl_2]^{+}$ is also likely to be present.

The uptake of lipophilic cations across phospholipid bilayers is largely determined by the balance between their charge and hydrophobicity (Ross et al., 2005). The charge raises the Born energy for movement into the bilayer, and this is counteracted by increasing hydrophobicity. Consequently, only relatively hydrophobic TPP-conjugated compounds with low charge are readily accumulated by mitochondria (Ross et al., 2005). MitoSOD was more lipophilic than the parent macrocycle M40403, as shown by their octanol/PBS partition coefficients of 2.2 ± 0.03 and 0.63 ± 0.03, respectively (n = 3, means ± SD). The MitoSOD partition coefficient is higher than that for many TPP monocations, such as TPMP (partition coefficient = 0.33), which is readily taken up into mitochondria, indicating that the monocation form of MitoSOD, $[Mn^{II}(L\text{-}TPP)Cl_2]^{+}$, should be taken up by energized mitochondria. The double charge on the dication form of MitoSOD, $[Mn^{II}(L\text{-}TPP)Cl]^{2+}$, raises its Born energy considerably, and studies of bisTPP dications have shown that they have to be more hydrophobic than the corresponding monocation to be taken up by mitochondria (Ross et al., 2006, 2005). As lipophilic TPP dications with a partition coefficient >0.8 are taken up (Ross et al., 2006), the doubly charged form of MitoSOD, $[Mn^{II}(L\text{-}TPP)Cl]^{2+}$, may be sufficiently hydrophobic to pass through the mitochondrial inner membrane. However, the form of MitoSOD present within the octanol phase may be the moncation, and consequently it is not possible to conclude from partition coefficient measurements alone that the MitoSOD dication is sufficiently hydrophobic to cross a biological membrane. We conclude that MitoSOD is stable to dissociation under typical biological pH and exists predominantly as $[Mn^{II}(L\text{-}TPP)Cl]^{2+}$ with small amounts of $[Mn^{II}(L\text{-}TPP)Cl_2]^{+}$. In addition, the monocation and possibly the dication are sufficiently hydrophobic to be taken up across biological membranes.

Uptake of MitoSOD by Energized Mitochondria

For MitoSOD to be an effective mitochondria-targeted SOD mimetic, it must be selectively accumulated by mitochondria in response to the membrane potential. To assess this, we used an ion-selective electrode that is responsive to lipophilic

TPP cations (Asin-Cayuela et al., 2004) and that responds to MitoSOD (Figure 4A). The electrode response was calibrated by additions of 1 to 5 μM MitoSOD, and then unenergized mitochondria were added, resulting in a lowering of the solution concentration of MitoSOD (Figure 4B). The observation of extensive binding of MitoSOD to the unenergized mitochondria is consistent with the behavior of other hydrophobic TPP cations (Asin-Cayuela et al., 2004). Addition of the respiratory substrate succinate generated a membrane potential across the inner membrane, leading to uptake of MitoSOD into the mitochondria, as indicated by its loss from the incubation medium, and this uptake was reversed when the uncoupler carbonyl cyanide-*p*-trifluoromethoxyphenylhydrazone (FCCP) was added to dissipate the membrane potential (Figure 4B). In this experiment ~9 nmol of MitoSOD was bound to the unenergized mitochondria, and on energization a further ~4.5 nmol of MitoSOD was taken up, corresponding to an intramitochondrial MitoSOD concentration of ~1.5 mM, assuming an intramitochondrial volume of 0.5 μl mg protein^{-1} (Brown and Brand, 1985). As the external concentration of MitoSOD at this point was then ~0.5 μM, this indicates an accumulation of approximately 3,000-fold, consistent with membrane potential-dependent uptake and binding of MitoSOD within mitochondria.

To further assess MitoSOD uptake by mitochondria and compare it with that of M40403, we next investigated the uptake of [^{3}H]MitoSOD and [^{3}H]M40403. When [^{3}H]MitoSOD was incubated with energized mitochondria, there was rapid and extensive uptake of MitoSOD into mitochondria that was stable for up to 15 min and was decreased by incubation with the uncoupler FCCP (Figure 4C). Conversely, when [^{3}H]M40403 was incubated with energized mitochondria, there was negligible accumulation of this macrocycle into the mitochondrial pellet (Figure 4C). The far greater uptake of MitoSOD over M40403 is consistent with its uptake into mitochondria in response to the membrane potential. Overall, by considering the interaction with unenergized mitochondria (Figure 4B), with uncoupled mitochondria (Figure 4C), and the value of its partition coefficient, it is clear that MitoSOD is extensively bound to unenergized mitochondria by adsorption to membranes. To better distinguish between simple binding and membrane potential-driven accumulation into mitochondria, we expressed the uptake of [^{3}H]MitoSOD into the pellet as an accumulation ratio (ACR: mol l^{-1} in mitochondria/mol l^{-1} in supernatant). This ACR of [^{3}H]MitoSOD was compared with that of [^{3}H]TPMP in parallel experiments over a range of mitochondrial membrane potentials set by different concentrations of the respiratory inhibitor malonate (Figure 4D) (Ross et al., 2008). As expected from Figures 4B and 4C, it is evident that with uncoupled mitochondria, there is extensive binding of MitoSOD, and as the membrane potential increases there is an increase in ACR. The maximal ACR for MitoSOD was found to be ~1,300, whereas the ACR for TPMP was ~550 under comparable conditions. Furthermore, when mitochondria were fully uncoupled with FCCP, the MitoSOD ACR was still significant at ~500. Together, these findings are consistent with extensive nonspecific binding of the hydrophobic MitoSOD to mitochondria. The slope of the plot of the ACR of MitoSOD against that of TPMP (Figure 4D) is greater than one, indicating that within mitochondria there is more extensive binding of MitoSOD to the matrix face of the inner membrane than for TPMP, as expected from its greater hydrophobicity (partition coefficient: MitoSOD, 2.2; TPMP, 0.33).

It is well established that the uptake of TPMP reflects the mitochondrial membrane potential and is satisfactorily described by the Nernst equation for a monocation. The uptake of MitoSOD (Figure 4D) is about twice that of TPMP. However, if MitoSOD crosses the membrane as a dication then, from the Nernst equation, its uptake would be expected to be orders of magnitude greater than that of TPMP (Ross et al., 2006). Furthermore, the ACR for MitoSOD is a linear function of that for TPMP, consistent with the uptake of MitoSOD as a monocation. Earlier we showed that the dication form of MitoSOD predominates in biological solutions. For a dication to be taken up across a phospholipid bilayer the high Born energy for transport due to the double charge must be balanced by elevated hydrophobicity. The octanol/PBS partition coefficient for MitoSOD was, by comparision with other lipohilic dications, sufficient for it to be taken up into mitochondria. However, a limitation to this comparision is that the form of MitoSOD that partitions into the octanol phase may be the monocation, in which case the dication form of MitoSOD may be too hydrophilic to pass through a phospholipid bilayer. This possibility, in conjunction with the data from Figure 4, lead us to conclude that MitoSOD is taken up by mitochondria in response to the membrane potential and, even though the dominant form of MitoSOD in solution is a dication, the monocation is likely to be the major form passing through the membrane bilayer.

For MitoSOD to be an effective SOD mimetic within mitochondria, it is important that it is taken up as the intact Mn(II) macrocycle. The apo form of MitoSOD, in which Mn has been removed by acid treatment, was found to be readily taken up by energized mitochondria (data not shown). Consequently, the uptake of MitoSOD as seen in Figure 4 could be explained by prior dissociation of Mn from MitoSOD, followed by uptake of apo-MitoSOD. To determine whether MitoSOD was accumulated intact, we measured, by inductively coupled plasma mass spectrometry, the extent of Mn uptake into mitochondria during incubations with MitoSOD. Incubation with 5 μM MitoSOD led to the rapid uptake of ~2.5–3.5 nmol Mn (Figure 5A), with similar kinetics and extent of uptake as seen for MitoSOD itself (Figure 4). To see if it was possible for apo-MitoSOD to be taken up by mitochondria and then incorporate Mn to form MitoSOD in situ, we incubated apo-MitoSOD with $MnCl_2$ and found no observable Mn incorporation to give MitoSOD, as assessed by mass spectrometry (Figure S2B). Incubation of apo-MitoSOD with mitochondria did not lead to MitoSOD assembly (data not shown), and incubation of apo-MitoSOD and $MnCl_2$ with mitochondria did not lead to uptake of Mn into mitochondria (Figure 5A). Therefore, we conclude that MitoSOD is taken up into mitochondria as an intact complex and the uptake of apo-MitoSOD alone does not lead to the assembly of MitoSOD within the mitochondrial matrix.

MitoSOD Protects Mitochondrial Aconitase from Superoxide Damage

To assess the ability of MitoSOD to detoxify $O_2^{\bullet-}$ within mitochondria, we used the redox cycler paraquat to induce $O_2^{\bullet-}$ formation in isolated heart mitochondria and monitored the $O_2^{\bullet-}$-dependent inactivation of the intramitochondrial enzyme

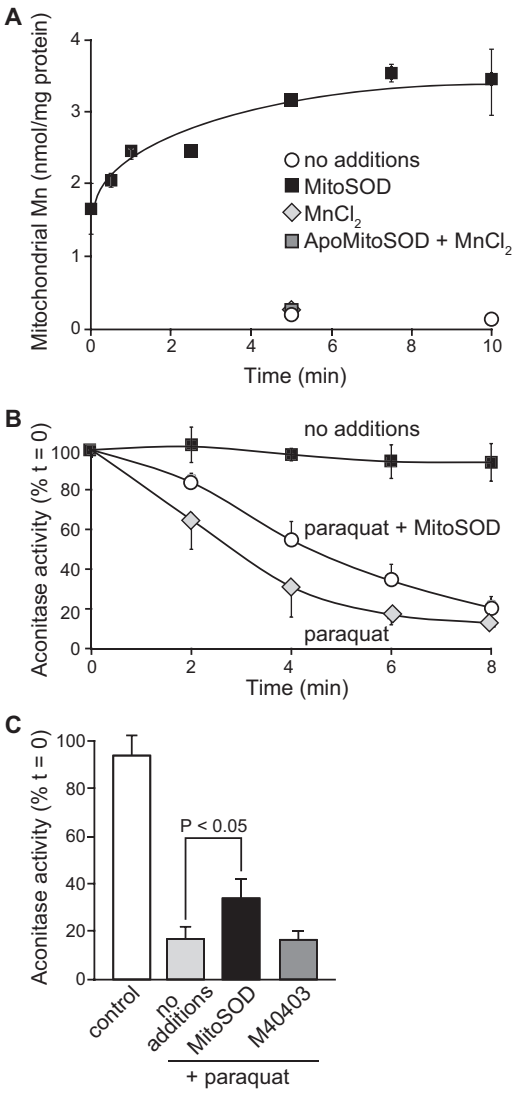

Figure 5. MitoSOD Increases Mitochondrial Mn Uptake and Decreases Aconitase Inactivation

Rat liver mitochondria (1 mg protein ml^{-1}) were incubated in 0.5 ml incubation medium supplemented with 10 mM succinate, 8 μg ml^{-1} rotenone at 37°C for the indicated times with 5 μM MitoSOD, no additions, 5 μM $MnCl_2$, or 1 μM apo-MitoSOD + 5 μM $MnCl_2$. Then the mitochondria were pelleted, and the concentration of Mn in the pellets was determined by inductively coupled plasma (ICP) analysis. Data are means ± SD of quadruplicate determinations.

(B) Rat heart mitochondria (2 mg protein ml^{-1}) were incubated in incubation medium (600–800 μl) containing glutamate/malate (10 mM) and bovine serum albumin (5% w/v), with or without paraquat (500 μM) or MitoSOD (5 μM) or M40403 (5 μM), at 37°C for the indicated times. Samples (100 μl), taken immediately before paraquat addition and at the indicated times were snap-frozen on dry ice and assessed for aconitase activity. Aconitase activity is expressed as a percentage of the activity immediately before paraquat addition. Data correspond to the means ± SD of three independent experiments.

(C) Mitochondria were incubated and processed as in (B) for 6 min with or without paraquat (500 μM), MitoSOD (5 μM), or M40403 (5 μM). Statistical significance was calculated by a two-tailed, paired Student's t test.

See also Figure S2.

aconitase, which is particularly sensitive to $O_2^{\bullet-}$ (Cochemé and Murphy, 2008). Paraquat decreased the activity of mitochondrial aconitase to 18% of control, and addition of MitoSOD partially protected aconitase from this damage (Figures 5B and 5C). In contrast, M40403 was ineffective, presumably because of its lack of uptake by mitochondria (Figure 5C). Although the extent of protection by MitoSOD is modest, this is expected because the rate constant of MitoSOD-catalyzed $O_2^{\bullet-}$ dismutation (5×10^6 M^{-1} s^{-1} at pH 8.0, 22°C) is ~400-fold lower than k_{cat} for the mitochondrial enzyme MnSOD (2×10^9 M^{-1} s^{-1} at 25°C; Bull et al., 1991). However, the large amount of MitoSOD taken up by mitochondria in response to the membrane potential (~1.5 mM) significantly increases the $O_2^{\bullet-}$ defense capacity, although as the concentration of MnSOD in the mitochondrial matrix is ~10–20 μM, the accumulated MitoSOD provides at most 20%–30% of the SOD activity in the mitochondrial matrix under these conditions. Higher concentrations of MitoSOD provided no further protection because at higher concentrations TPP cations start to affect the membrane potential, thereby limiting further accumulation.

SIGNIFICANCE

Antioxidants targeted to mitochondria by conjugation to lipophilic cations have proven useful as tools for investigating oxidative damage and redox signaling, and as potential therapies for diseases involving mitochondrial oxidative damage (Murphy and Smith, 2007, 2010). Although some mitochondria-targeted antioxidants can react with $O_2^{\bullet-}$, they are not selective. Consequently, it is not possible to infer if their action is due to depleting $O_2^{\bullet-}$ or to some other antioxidant reaction. We have resolved this issue by inventing a mitochondria-targeted antioxidant that is selective for $O_2^{\bullet-}$. This was achieved by conjugating the core functionality of the Mn(II) macrocycle SOD mimetic M40403 to the mitochondria-targeting lipophilic cation TPP. The resultant compound, MitoSOD, was a very effective catalytic SOD mimetic and also had catalytic $O_2^{\bullet-}$ reductase activity in the presence of the biological reductant ascorbate. The rate constant of MitoSOD-catalyzed $O_2^{\bullet-}$ dismutation (5×10^6 M^{-1} s^{-1} at pH 8.0, 22°C) is lower than k_{cat} for the mitochondrial enzyme MnSOD (2×10^9 M^{-1} s^{-1} at 25°C; Bull et al., 1991). However, the large amount of MitoSOD taken up by mitochondria in response to the membrane potential significantly increases the $O_2^{\bullet-}$ defense capacity within mitochondria above that provided by the endogenous MnSOD enzyme alone, indicating that this is a viable antioxidant strategy and that developing analogs of MitoSOD with greater rates of $O_2^{\bullet-}$ dismutation is the best path to development of future SOD mimetics. To our knowledge, MitoSOD constitutes the first example of a selective macrocyclic Mn(II) SOD mimetic that is taken up into mitochondria, driven by the membrane potential, and exhibits a protective effect against $O_2^{\bullet-}$ within mitochondria. This work establishes the baseline parameters for the rational development of bioactive mitochondria-targeted SOD mimetics, as well as other mitochondria-targeted macrocycle and metal-dependent moieties, with potential for pharmaceutical application.

EXPERIMENTAL PROCEDURES

Synthetic Chemistry

The target compounds MitoSOD (**1**) and M40403 (**2**) were obtained by Mn(II) template cyclization of the tetraamine **3** and **4** or 2,6-pyridinedialdehyde, respectively, followed by in situ borohydride reduction of the intermediate Schiff-base macrocycle (Figure 1A). General synthetic methods and details of syntheses are given in the Supplemental Experimental Procedures.

X-Ray Crystallography

X-ray data were collected by Assoc. Prof. C.E.F. Rickard, The University of Auckland, New Zealand, on a Bruker SMART diffractometer using graphite-monochromated Mo-Kα radiation (λ = 0.71073 Å). MitoSOD crystallized in the chiral monoclinic space group $P2_1$ with one molecule of coordinated water and two half occupancy noncoordinated molecules of ethanol per $MnLCl_3$, that is, as $[MnLCl(OH_2)]Cl_2 \cdot EtOH$. The data were corrected for Lorentz and polarization effects, and a semiempirical absorption correction (SADABS) was applied. The structure was solved by direct methods (SHELXS-97) (Sheldrick, 1990, 1997) and refined using SHELXL-97 (Sheldrick and Schneider, 1997). All nonhydrogen atoms were made anisotropic. Hydrogen atoms were inserted at calculated positions and rode on the atoms to which they are attached, except for those on N2, N3, N4, N5, and O1, which were located from difference maps and fixed (AFIX 01). The two half occupancy EtOH solvent molecules are both well behaved. One of the two noncoordinating chloride ions is modeled as disordered over two sites as 0.85:0.15 Cl2:Cl2′ (an attempt to model this as a Cl:Br disorder resulted in 0.9:0.1 occupancy; this option, of the presence of a trace of Br, cannot be excluded although it was not employed here). Mn(II) is coordinated by the five N atoms of the macrocycle in a near-planar arrangement, as evident from the sum of the five N-Mn-N chelate angles (363°). A chloride ion and water molecule are also coordinated to Mn(II), with a Cl⁻Mn-O angle of 176.8°; the geometry of the coordination sphere is best described as pentagonal bipyramidal. The alternating axial disposition of the cyclohexyl methine hydrogens confirmed the stereochemistry of the four chiral centers of the macrocycle. Despite the existence of M40403 being known for at least a decade, its X-ray structure remains unreported. An attempt by us to prepare crystals of M40403 resulted in crystal twinning, and an X-ray structure was unable to be obtained. Hence, the MitoSOD structure was compared to the X-ray structure of a pentagonal bipyramidal polymorph of M40401, an active 1,1′-(pyridine-2,6-diyl)diethanamine analog of M40403 (Aston et al., 2001). The MitoSOD and M40401 structures showed similar Mn-N bond lengths and N-Mn-N chelate angles.

Pulse Radiolysis

The 4 MeV linear accelerator (LINAC) of The University of Auckland, New Zealand, was used to irradiate sample solutions contained in a quartz cuvette. The LINAC has been adapted to produce variable amounts of radiation (0–100 Gy in 1.5 μs) to the sample. Dosimetry was carried out using aerated KSCN solution assuming the $(SCN)_2^{\bullet-}$ radical produced has a radiation chemical yield (G) of 0.29 μM Gy^{-1} and an extinction coefficient of 7,580 M^{-1} cm^{-1} at 475 nm (Schuler et al., 1980). Changes in absorbance were measured using a PC-controlled custom-built optical detection system (Anderson et al., 1997). All experiments were performed at 22°C ± 1°C.

The radiolysis of water with high-energy electrons produces both primary radical species and products as shown in Equation (1). The G-values of the different species (in μM Gy^{-1}) are shown in parentheses.

$$H_2O \rightsquigarrow e_{aq}^-(0.28) + {}^{\bullet}OH(0.28) + {}^{\bullet}H(0.055) + H_2(0.04) + H_2O_2(0.07) + H_3O^+(0.28) \quad (1)$$

Quantitative amounts of $O_2^{\bullet-}$ were produced in aerated solutions containing sodium formate (10 mM), phosphate buffer (10 mM [pH 7.4 or 8.0]), and EDTA (0.1 mM). Under these conditions, all the primary radical species are quickly converted into $O_2^{\bullet-}$, as described by Equations (2)–(7), resulting in a yield of $O_2^{\bullet-}$ of 0.62 μM Gy^{-1} by the end of the pulse (Bielski et al., 1985; Ilan and Rabani, 1976).

$$O_2 + e_{aq}^- \rightarrow O_2^{\bullet-} \quad k = 1.9 \times 10^{10}\ M^{-1}\ s^{-1}, \quad (2)$$

$$O_2 + H^{\bullet} \rightarrow HO_2^{\bullet} \quad k = 1.2 \times 10^{10}\ M^{-1}\ s^{-1}, \quad (3)$$

$$HO_2\cdot \leftrightharpoons H^+ + O_2^{\bullet-}, \quad (4)$$

$$HCO_2^- + HO\cdot \rightarrow CO_2^{\bullet-} + H_2O \quad k = 3.2 \times 10^9\ M^{-1}\ s^{-1}, \quad (5)$$

$$HCO_2^- + H\cdot \rightarrow CO_2^{\bullet-} + H_2 \quad k = 2.1 \times 10^8\ M^{-1}\ s^{-1}, \quad (6)$$

$$O_2 + CO_2^{\bullet-} \rightarrow O_2^{\bullet-} + CO_2 \quad k = 4.2 \times 10^9\ M^{-1}\ s^{-1}. \quad (7)$$

The decay in the optical absorbance due to $O_2^{\bullet-}$, for various radiation doses, was monitored at 270 nm, and the first half-lives were obtained directly from the absorbance traces.

Determination of SOD Activity

For Figures 3A and 3B, a mixture of acetylated ferricytochrome c (25 μM) in potassium phosphate (50 mM) and EDTA (100 μM) at pH 7.8 was supplemented with hypoxanthine (50 μM), held at 25°C in a 1 ml cuvette, and the absorbance at 550 nm was monitored (Loschen et al., 1974). After 30 s incubation, $O_2^{\bullet-}$ production was initiated by addition of xanthine oxidase (XO, 0.2 U ml^{-1}) to give an $O_2^{\bullet-}$ generation rate of ~6 μM min^{-1}, and then after a further 90 s the test compounds were added from a DMSO stock solution. The rate of cytochrome c reduction at 550 nm was recorded for a further 3 min. Monitoring the formation of uric acid at 295 nm confirmed that MitoSOD up to at least 10 μM did not inhibit XO activity. Demetallation of MitoSOD by treatment with acid gave a metal-free residue that had no SOD activity. The comparison of the specific SOD activity for Cu,ZnSOD, MitoSOD, and M40403 was assessed by the WST-1 assay as described (Peskin and Winterbourn, 2000). For Figure 3C, ascorbate oxidation and cytochrome c reduction were measured at 22°C in 50 mM phosphate buffer (pH 7.4) containing 50 μM DTPA and 5 μg ml^{-1} catalase. A flux of $O_2^{\bullet-}$ was generated by addition of XO (~0.1 U ml^{-1} to give a $O_2^{\bullet-}$ generation rate of 2 μM min^{-1}) and acetaldehyde (10 mM). Cu,ZnSOD (60 nM), or various concentrations of M40403 and MitoSOD, was added to this. Then either cytochrome c (20 μM) was added and its rate of reduction was monitored at 550 nm, or ascorbate (30 μM) was added and its rate of oxidation was monitored at 266 nm. Data are means ± ranges for 2–3 determinations. The oxidation rate of ascorbate alone, which was ~2% of the $O_2^{\bullet-}$-dependent reaction, was subtracted.

Uptake of MitoSOD by Mitochondria

An ion-selective electrode was prepared that responds to the triphenylphosphonium (TPP) moiety (Asin-Cayuela et al., 2004) and inserted into a stirred solution of incubation medium (120 mM KCl, 10 mM HEPES [pH 7.2], and 1 mM EGTA). The uptake of [^{3}H]MitoSOD and [^{3}H]M40403 by isolated rat liver mitochondria (1 mg protein ml^{-1}) was determined by suspension in Incubation Medium supplemented with 10 mM succinate, 8 μg ml^{-1} rotenone, 4 μM MitoSOD or M40403, and 1 μM [^{3}H]MitoSOD (28 Ci mol^{-1}) or [^{3}H]-M40403 (13 Ci mol^{-1}) at 25°C. The uptake of [^{3}H]MitoSOD and [^{3}H]M40403 was determined at various times by isolating the mitochondria by centrifugation and then determining the amount of [^{3}H]macrocycle in the mitochondrial pellet by scintillation counting and using the specific activity of the starting solution to calculate the amount associated with the mitochondria (Kelso et al., 2001; Smith et al., 1999, 2004). The data are means of three separate experiments ± SEM. For the FCCP experiment, 500 nM FCCP was present. To determine the effect of the mitochondrial membrane potential on the uptake of [^{3}H]-MitoSOD rat liver mitochondria (1 mg protein ml^{-1}) were incubated in incubation medium containing 10 mM succinate, 8 μg ml^{-1} rotenone, 100 μg ml^{-1} nigericin, 800 nM MitoSOD, 1 μM TPMP, and 1–16 mM malonate, or to measure the uptake of ^{3}H-labeled compounds in the complete absence of a membrane potential, FCCP (330 nM) was added to the incubation medium. These were supplemented with either 200 nM [^{3}H]MitoSOD (28 Ci mol^{-1}) or 100 nM [^{3}H]TPMP (500 Ci mol^{-1}) for 3 min at 25°C. The ACR of [^{3}H]MitoSOD or [^{3}H]TPMP was determined at various times in parallel to enable the ACR for the two compounds to be determined under identical conditions by isolating the mitochondria by centrifugation and then determining the amount of [^{3}H]MitoSOD or [^{3}H]TPMP in the mitochondrial pellet and in the supernatant by scintillation counting and taking the mitochondrial volume as 0.5 μl mg protein^{-1}.

Determination of Aconitase Activity

Aliquots (10 μl) of the snap-frozen mitochondrial incubtions samples were incubated in assay buffer (190 μl) comprising Tris-HCl (50 mM [pH 7.4]), $MnCl_2$ (0.6 mM), sodium citrate (5 mM [pH 7.0]), $NADP^+$ (0.2 mM), Triton X-100 (0.1% v/v), and isocitrate dehydrogenase (0.4 U ml^{-1}) in quintuplicate at 30°C in a 96-well plate, and the appearance of NADPH ($\varepsilon_{340} = 6.22 \times 10^3$ M^{-1} cm^{-1}) was monitored over 10 min at 340 nm (Cochemé and Murphy, 2008).

SUPPLEMENTAL INFORMATION

Supplemental Information includes two figures, three tables, and Supplemental Experimental Procedures and can be found with this article online at http://dx.doi.org/10.1016/j.chembiol.2012.08.005.

ACKNOWLEDGMENTS

This work was supported by Grant UOA 0407 of the Marsden Fund from the Royal Society of New Zealand and by the Medical Research Council (UK).

Received: May 30, 2012
Revised: July 27, 2012
Accepted: August 4, 2012
Published: October 25, 2012

REFERENCES

Anderson, R.F., Denny, W.A., Li, W., Packer, J.E., Tercel, M., and Wilson, W.R. (1997). Pulse radiolysis studies on the fragmentation of arylmethyl quaternary nitrogen mustards by one-electron reduction in aqueous solution. J. Phys. Chem. A *101*, 9704–9709.

Anderson, R.F., Shinde, S.S., Hay, M.P., Gamage, S.A., and Denny, W.A. (2003). Activation of 3-amino-1,2,4-benzotriazine 1,4-dioxide antitumor agents to oxidizing species following their one-electron reduction. J. Am. Chem. Soc. *125*, 748–756.

Asin-Cayuela, J., Manas, A.R., James, A.M., Smith, R.A., and Murphy, M.P. (2004). Fine-tuning the hydrophobicity of a mitochondria-targeted antioxidant. FEBS Lett. *571*, 9–16.

Aston, K., Rath, N., Naik, A., Slomczynska, U., Schall, O.F., and Riley, D.P. (2001). Computer-aided design (CAD) of Mn(II) complexes: superoxide dismutase mimetics with catalytic activity exceeding the native enzyme. Inorg. Chem. *40*, 1779–1789.

Batinić-Haberle, I. (2002). Manganese porphyrins and related compounds as mimics of superoxide dismutase. Methods Enzymol. *349*, 223–233.

Batinić-Haberle, I., Rebouças, J.S., and Spasojević, I. (2010). Superoxide dismutase mimics: chemistry, pharmacology, and therapeutic potential. Antioxid. Redox Signal. *13*, 877–918.

Bielski, B.H.J., Cabelli, D.E., and Arudi, R. (1985). Reactivity of $HO_2^{\bullet}/O_2^{\bullet-}$ radicals in aqueous solution. J. Phys. Chem. Ref. Data *14*, 1041–1100.

Brown, G.C., and Brand, M.D. (1985). Thermodynamic control of electron flux through mitochondrial cytochrome bc1 complex. Biochem. J. *225*, 399–405.

Brown, S.E., Ross, M.F., Sanjuan-Pla, A., Manas, A.R., Smith, R.A., and Murphy, M.P. (2007). Targeting lipoic acid to mitochondria: synthesis and characterization of a triphenylphosphonium-conjugated alpha-lipoyl derivative. Free Radic. Biol. Med. *42*, 1766–1780.

Bull, C., Niederhoffer, E.C., Yoshida, T., and Fee, J.A. (1991). Kinetic studies of superoxide dismutases: properties of the manganese-containing protein from Thermus thermophilus. J. Am. Chem. Soc. *113*, 4069–4076.

Cadenas, E., and Davies, K.J. (2000). Mitochondrial free radical generation, oxidative stress, and aging. Free Radic. Biol. Med. *29*, 222–230.

Chen, Z., Siu, B., Ho, Y.S., Vincent, R., Chua, C.C., Hamdy, R.C., and Chua, B.H. (1998). Overexpression of MnSOD protects against myocardial ischemia/reperfusion injury in transgenic mice. J. Mol. Cell. Cardiol. *30*, 2281–2289.

Cochemé, H.M., and Murphy, M.P. (2008). Complex I is the major site of mitochondrial superoxide production by paraquat. J. Biol. Chem. *283*, 1786–1798.

Collins, Y., Chouchani, E.T., James, A.M., Menger, K.E., Cochemé, H.M., and Murphy, M.P. (2012). Mitochondrial redox signalling at a glance. J. Cell Sci. *125*, 801–806.

Dessolin, J., Schuler, M., Quinart, A., De Giorgi, F., Ghosez, L., and Ichas, F. (2002). Selective targeting of synthetic antioxidants to mitochondria: towards a mitochondrial medicine for neurodegenerative diseases? Eur. J. Pharmacol. *447*, 155–161.

Dhanasekaran, A., Kotamraju, S., Karunakaran, C., Kalivendi, S.V., Thomas, S., Joseph, J., and Kalyanaraman, B. (2005). Mitochondria superoxide dismutase mimetic inhibits peroxide-induced oxidative damage and apoptosis: role of mitochondrial superoxide. Free Radic. Biol. Med. *39*, 567–583.

Dikalova, A.E., Bikineyeva, A.T., Budzyn, K., Nazarewicz, R.R., McCann, L., Lewis, W., Harrison, D.G., and Dikalov, S.I. (2010). Therapeutic targeting of mitochondrial superoxide in hypertension. Circ. Res. *107*, 106–116.

Doctrow, S.R., Huffman, K., Marcus, C.B., Musleh, W., Bruce, A., Baudry, M., and Malfroy, B. (1997). Salen-manganese complexes: combined superoxide dismutase/catalase mimics with broad pharmacological efficacy. Adv. Pharmacol. *38*, 247–269.

Faulkner, K.M., Liochev, S.I., and Fridovich, I. (1994). Stable Mn(III) porphyrins mimic superoxide dismutase in vitro and substitute for it *in vivo*. J. Biol. Chem. *269*, 23471–23476.

Feltham, R.D., and Hayter, R.G. (1964). The electrolyte type of ionized complexes. J. Chem. Soc., *0*, 4587–4591.

Filipović, M.R., Duerr, K., Mojović, M., Simeunović, V., Zimmermann, R., Niketić, V., and Ivanović-Burmazović, I. (2008). NO dismutase activity of seven-coordinate manganese(II) pentaazamacrocyclic complexes. Angew. Chem. Int. Ed. Engl. *47*, 8735–8739.

Filipović, M.R., Koh, A.C., Arbault, S., Niketić, V., Debus, A., Schleicher, U., Bogdan, C., Guille, M., Lemaître, F., Amatore, C., and Ivanović-Burmazović, I. (2010). Striking inflammation from both sides: manganese(II) pentaazamacrocyclic SOD mimics act also as nitric oxide dismutases: a single-cell study. Angew. Chem. Int. Ed. Engl. *49*, 4228–4232.

Filipovska, A., Kelso, G.F., Brown, S.E., Beer, S.M., Smith, R.A., and Murphy, M.P. (2005). Synthesis and characterization of a triphenylphosphonium-conjugated peroxidase mimetic. Insights into the interaction of ebselen with mitochondria. J. Biol. Chem. *280*, 24113–24126.

Finkel, T. (2005). Radical medicine: treating ageing to cure disease. Nat. Rev. Mol. Cell Biol. *6*, 971–976.

Friedel, F.C., Lieb, D., and Ivanović-Burmazović, I. (2012). Comparative studies on manganese-based SOD mimetics, including the phosphate effect, by using global spectral analysis. J. Inorg. Biochem. *109*, 26–32.

Gane, E.J., Weilert, F., Orr, D.W., Keogh, G.F., Gibson, M., Lockhart, M.M., Frampton, C.M., Taylor, K.M., Smith, R.A., and Murphy, M.P. (2010). The mitochondria-targeted anti-oxidant mitoquinone decreases liver damage in a phase II study of hepatitis C patients. Liver Int. *30*, 1019–1026.

Gotoh, N., and Niki, E. (1992). Rates of interactions of superoxide with vitamin E, vitamin C and related compounds as measured by chemiluminescence. Biochim. Biophys. Acta *1115*, 201–207.

Ilan, Y., and Rabani, J. (1976). Some fundamental reactions in radiation-chemistry: nanosecond pulse radiolysis. Int. J. Radiat. Phys. Chem. *8*, 609–611.

Iranzo, O. (2011). Manganese complexes displaying superoxide dismutase activity: a balance between different factors. Bioorg. Chem. *39*, 73–87.

Kagan, V.E., Jiang, J., Bayir, H., and Stoyanovsky, D.A. (2007). Targeting nitroxides to mitochondria: location, location, location, and ...concentration: highlight commentary on "Mitochondria superoxide dismutase mimetic inhibits peroxide-induced oxidative damage and apoptosis: role of mitochondrial superoxide". Free Radic. Biol. Med. *43*, 348–350.

Kelso, G.F., Porteous, C.M., Coulter, C.V., Hughes, G., Porteous, W.K., Ledgerwood, E.C., Smith, R.A.J., and Murphy, M.P. (2001). Selective targeting of a redox-active ubiquinone to mitochondria within cells: antioxidant and antiapoptotic properties. J. Biol. Chem. *276*, 4588–4596.

Kim, A., Zhong, W., and Oberley, T.D. (2004). Reversible modulation of cell cycle kinetics in NIH/3T3 mouse fibroblasts by inducible overexpression of mitochondrial manganese superoxide dismutase. Antioxid. Redox Signal. *6*, 489–500.

Li, X., Cobb, C.E., Hill, K.E., Burk, R.F., and May, J.M. (2001). Mitochondrial uptake and recycling of ascorbic acid. Arch. Biochem. Biophys. *387*, 143–153.

Loschen, G., Azzi, A., Richter, C., and Flohé, L. (1974). Superoxide radicals as precursors of mitochondrial hydrogen peroxide. FEBS Lett. *42*, 68–72.

Maroz, A., Kelso, G.F., Smith, R.A., Ware, D.C., and Anderson, R.F. (2008). Pulse radiolysis investigation on the mechanism of the catalytic action of Mn(II)-pentaazamacrocycle compounds as superoxide dismutase mimetics. J. Phys. Chem. A *112*, 4929–4935.

Murphy, M.P. (2009). How mitochondria produce reactive oxygen species. Biochem. J. *417*, 1–13.

Murphy, M.P., and Smith, R.A. (2007). Targeting antioxidants to mitochondria by conjugation to lipophilic cations. Annu. Rev. Pharmacol. Toxicol. *47*, 629–656.

Murphy, M.P., Echtay, K.S., Blaikie, F.H., Asin-Cayuela, J., Cocheme, H.M., Green, K., Buckingham, J.A., Taylor, E.R., Hurrell, F., Hughes, G., et al. (2003). Superoxide activates uncoupling proteins by generating carbon-centered radicals and initiating lipid peroxidation: studies using a mitochondria-targeted spin trap derived from alpha-phenyl-N-tert-butylnitrone. J. Biol. Chem. *278*, 48534–48545.

Peskin, A.V., and Winterbourn, C.C. (2000). A microtiter plate assay for superoxide dismutase using a water-soluble tetrazolium salt (WST-1). Clin. Chim. Acta *293*, 157–166.

Ross, M.F., Kelso, G.F., Blaikie, F.H., James, A.M., Cochemé, H.M., Filipovska, A., Da Ros, T., Hurd, T.R., Smith, R.A., and Murphy, M.P. (2005). Lipophilic triphenylphosphonium cations as tools in mitochondrial bioenergetics and free radical biology. Biochemistry (Mosc.) *70*, 222–230.

Ross, M.F., Da Ros, T., Blaikie, F.H., Prime, T.A., Porteous, C.M., Severina, I.I., Skulachev, V.P., Kjaergaard, H.G., Smith, R.A., and Murphy, M.P. (2006). Accumulation of lipophilic dications by mitochondria and cells. Biochem. J. *400*, 199–208.

Ross, M.F., Prime, T.A., Abakumova, I., James, A.M., Porteous, C.M., Smith, R.A.J., and Murphy, M.P. (2008). Rapid and extensive uptake and activation of hydrophobic triphenylphosphonium cations within cells. Biochem. J. *411*, 633–645.

Salvemini, D., Wang, Z.-Q., Zweier, J.L., Samouilov, A., Macarthur, H., Misko, T.P., Currie, M.G., Cuzzocrea, S., Sikorski, J.A., and Riley, D.P. (1999). A nonpeptidyl mimic of superoxide dismutase with therapeutic activity in rats. Science *286*, 304–306.

Salvemini, D., Riley, D.P., and Cuzzocrea, S. (2002). SOD mimetics are coming of age. Nat. Rev. Drug Discov. *1*, 367–374.

Schuler, R.H., Patterson, L.K., and Janata, E. (1980). Yield for the scavenging of hydroxyl radicals in the radiolysis of N2O-saturated aqueous solutions. J. Phys. Chem. *84*, 2088–2089.

Sheldrick, G.M. (1990). Phase annealing in SHELX-90: direct methods for larger structures. Acta Cryst. *A46*, 467–473.

Sheldrick, G.M. (1997). Patterson superposition and ab initio phasing. In Macromolecular Crystallography, Pt A, C. Carter, Jr. and R. Sweet, eds. (San Diego: Academic Press), pp. 628–641.

Sheldrick, G.M., and Schneider, T.R. (1997). SHELXL: high-resolution refinement. In Macromolecular Crystallography, Pt B, C. Carter, Jr. and R. Sweet, eds. (San Diego: Academic Press), pp. 319–343.

Skulachev, V.P., Anisimov, V.N., Antonenko, Y.N., Bakeeva, L.E., Chernyak, B.V., Erichev, V.P., Filenko, O.F., Kalinina, N.I., Kapelko, V.I., Kolosova, N.G., et al. (2009). An attempt to prevent senescence: a mitochondrial approach. Biochim. Biophys. Acta *1787*, 437–461.

Smith, R.A., and Murphy, M.P. (2010). Animal and human studies with the mitochondria-targeted antioxidant MitoQ. Ann. N Y Acad. Sci. *1201*, 96–103.

Smith, R.A., Kelso, G.F., James, A.M., and Murphy, M.P. (2004). Targeting coenzyme Q derivatives to mitochondria. Methods Enzymol. *382*, 45–67.

Smith, R.A., Hartley, R.C., and Murphy, M.P. (2011). Mitochondria-targeted small molecule therapeutics and probes. Antioxid. Redox Signal. *15*, 3021–3038.

Smith, R.A.J., Porteous, C.M., Coulter, C.V., and Murphy, M.P. (1999). Selective targeting of an antioxidant to mitochondria. Eur. J. Biochem. *263*, 709–716.

Snow, B.J., Rolfe, F.L., Lockhart, M.M., Frampton, C.M., O'Sullivan, J.D., Fung, V., Smith, R.A., Murphy, M.P., and Taylor, K.M.; Protect Study Group. (2010). A double-blind, placebo-controlled study to assess the mitochondria-targeted antioxidant MitoQ as a disease-modifying therapy in Parkinson's disease. Mov. Disord. *25*, 1670–1674.

Soule, B.P., Hyodo, F., Matsumoto, K., Simone, N.L., Cook, J.A., Krishna, M.C., and Mitchell, J.B. (2007). The chemistry and biology of nitroxide compounds. Free Radic. Biol. Med. *42*, 1632–1650.

Thompson, J.S., Chu, Y., Glass, J., Tapp, A.A., and Brown, S.A. (2010). The manganese superoxide dismutase mimetic, M40403, protects adult mice from lethal total body irradiation. Free Radic. Res. *44*, 529–540.

Trnka, J., Blaikie, F.H., Smith, R.A.J., and Murphy, M.P. (2008). A mitochondria-targeted nitroxide is reduced to its hydroxylamine by ubiquinol in mitochondria. Free Radic. Biol. Med. *44*, 1406–1419.

